THE JOURNAL OF PHYSICAL CHEMISTRY B

Article

pubs.acs.org/JPCB

Examination of CO_2−SO_2 Solubility in Water by SAFT1. Implications for CO_2 Transport and Storage

R. Miri,* P. Aagaard, and H. Hellevang*

Department of Geosciences, University of Oslo, Pb. 1047, Blindern, NO-0316 Oslo Norway

ABSTRACT: Removal of toxic gases like SO_2 by cosequestration with CO_2 in deep saline aquifers is a very attractive suggestion from environmental, human health and economic point of view. Examination of feasibility of this technique and forecasting the underlying fluid−rock interactions requires precise knowledge about the phase equilibria of the ternary mixture of SO_2−CO_2−H_2O at conditions relevant to carbon capture and storage (CCS). In this study, a molecular-based statistical association fluid theory (SAFT1) model is applied to estimate the phase equilibria and aqueous phase density of mixtures. The molecules are modeled as associating segments while self-association is not allowed. The model is tested for different SO_2 concentrations and for temperatures and pressures varying between 30−100 °C and ∼6−30 MPa, respectively. Comparison of the results of this model against the available experimental data of binary systems demonstrates the capability of this equation of state, although, in contrast to the previous works, no temperature dependent binary interaction coefficient is applied. The results show that the total solubility of SO_2 + CO_2 in water varies exponentially with respect to SO_2 concentrations, i.e., at low concentrations of SO_2, total changes in solubility of the CO_2 in water is negligible.

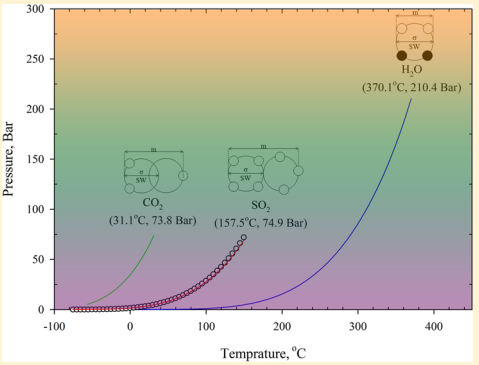

1. INTRODUCTION

Since industrial revolution, atmospheric CO_2 concentration has continuously increased to ∼397 ppmv and under a "business-as-usual" energy scenario, it is expected that throughout the coming centuries, this value may reach ∼750 ppmv.[1] Increasing concentrations of atmospheric CO_2 would result in a positive radiative forcing, which tends to increase the surface temperature of the Earth.[2] The IPCC Working Group I has proposed a set of pathways to stabilize the atmospheric CO_2 concentration at 450, 550, and 750 ppmv over the next hundred years.[1] To do so, out of the several mitigation options, carbon capture and storage (CCS) in geological reservoirs—especially saline aquifers—is recognized as the best solution with respect to mitigation potential.[3] A typical CSS project consist of three connected processes, including the separation of CO_2 from large industrial point sources, compression and transport to the storage cite, and injection in geological formation with the intention of long-term isolation from the atmosphere.[4,5]

The capture and separation stage will determine the composition of the transported and injected fluid. It is very often that an injected CO_2 stream contains some "impurities" which have different source and origins.[6−9] Some of the impurities, such SO_2, NO_2, H_2S, and H_2O, may be retained from a flue-gas capture and combustion phase and some, like light hydrocarbons (e.g., CH_4), are mixed with the injected CO_2 stream deep in the well. Complete separation of theses impurities is in some cases not economically feasible. Beside this, emission of some toxic impurities is hazardous from environmental and human health point of view.[7] Therefore, coinjection of toxic gases together with CO_2 in deep geological formation aquifers is an appealing solution toward this issue. This study focuses on sulfur dioxide (SO_2) as one of the major environmental pollutant and less addressed impurities in the CO_2 stream. Sulfur dioxide has very high solubility in water and is considered to be a highly corrosive compound under atmospheric conditions. Knowledge of phase equilibria of CO_2 + SO_2 mixture is necessary for both CCS processes and enhanced oil recovery (EOR). CO_2 at supercritical state has a considerable solubility in oil, and hence is traditionally used as a miscible displacement agent. On the other hand, lowering the minimum miscibility pressure, inclusion of sulfur dioxide will yield in a better swipe efficiency and higher recovery factor. With respect to CCS process, SO_2 might affect very much the transportation efficiency, geo-chemistry of the fluid−rock system, and even operational concerns like injectivity.

There are many uncertainties regarding coinjection of acid gases like SO_2, for example: What will be the fate of injected SO_2? How will the solubility of CO_2 and aqueous phase density change with respect to certain amount of SO_2? In what way and how will SO_2 affect the overall chemistry of the CO_2−rock system? How and to what degree will the efficiency of the transportation and CO_2 injectivity be altered? Knowledge of thermodynamic properties and phase equilibria of CO_2−SO_2−H_2O mixtures is necessary to answer these questions. For instance, pressure−temperature diagrams of CO_2−SO_2 would be very useful to avoid phase splits during transportation and to design the whole process in supercritical condition. Moreover,

Received: June 5, 2014
Revised: July 15, 2014
Published: July 15, 2014

   dx.doi.org/10.1021/jp505562j | J. Phys. Chem. B 2014, 118, 10214−10223

prediction of density of this binary mixture at supercritical condition is essential for estimation of storage capacity as well as gas injectivity. To the best of our knowledge, only one set of experimental data on this ternary mixture is reported in the literature,[10] and in the case of SO_2 associated binaries, only a few have been performed.[11−13]

On the modeling part, in spite of its importance, only a few studies have been performed. Li and Yan[14] have compared five different type of cubic equation of states (PR, SRK, RK, PT, 3P1T) to calculate the pressure−temperature diagrams of the CO_2−SO_2 mixture. Their result showed that the 3P1T EOS has the best performance for this system. Donget al.[15] incorporated perturbed-chain statistical associating fluid theory (PC-SAFT) and density-gradient theory (DGT) to estimate the bulk and interfacial properties of the CO_2−SO_2 mixture. They have used a constant binary interaction coefficient to fit their model against experimental data. Ziabakhsh-Ganjiet al.[9] used the Peng−Robinson (PR) theory coupled with a pressure adjusted form of the Henry constant and estimated the solubility of the SO_2 + CO_2 in water. Tanet al.[8] recently compared the capability of eCPA and PC-SAFT/PMSA for modeling of SO_2 + CO_2 in water. The results showed that at higher pressures PC-SAFT/PMSA noticeably outperforms eCPA. However, a three parameter temperature dependent binary interaction coefficient was used to fit the cross association parameters of the models against experimental data. Taking into account the lack of experimental data for H_2O + SO_2 + CO_2 mixture as well as wide range of temperature−pressure encountered during CCS, a reliable and predictive model and preferentially with a minimum of adjustable parameters is needed.

In general, two approaches are frequently used to model the equilibrium between two phases: the ϕ−ϕ approach and the γ−ϕ approach. These two approaches are characteristically equivalent and practical constrains of the problem determine that which method should be utilized. However, using a single equation of state for both phases (i.e. the ϕ−ϕ approach) is much more feasible computationally. In the γ−ϕ approach, the fugacity of the low-density vapor phase is calculated using an EoS and the activity coefficient models is commonly used for the liquid phase, which treats the nonideality as a chemical reaction. In spite of applicability of these models for polar and associating mixtures, however, they are valid only at moderate pressures. Cubic EoS such as Peng−Robinson (PR) and Soave−Redlich−Kwong (SRK) are traditional methods that use the ϕ−ϕ approach for phase equilibria calculations at high-pressure. However, the predictability and reliability of these semiempirical methods for polar and association molecules (complex fluids like H_2O + SO_2 + CO_2 mixture) is very poor due to their inherent deficiency in incorporating nonideal mixing.

Statistical association fluid theory (SAFT)[16−18] is a prevailing ϕ−ϕ approach for modeling of complex fluids, which was developed based on the molecular principles and by incorporating Wertheim's thermodynamic perturbation theory of the first order (TPT1). SAFT is built on a reference term which unlike van der Waals equations makes it able to capture chain length (molecular shape) and molecular association. The SAFT type EoS has been applied extensively in the literature to hydrocarbons mixtures,[19−21] ionic liquids,[22−24] polymers,[19,25,26] and solubility of gas and even solid components like slat or sugar in liquids.[27−29] Adidharmaet al.[19] introduced SAFT1 which has promising ability in representation of pure component properties over a wide density range—due to the correction applied to the dispersion term. The model incorporates square-well (SW) fluid potentials and formulated as to be applied for both homo and heterosegmented molecules. Lafitteet al.[30,31] used Mie potentials(which for exponents 12 and 6 also included Lennard−Jones potential) in the SAFT-VR framework (statistical associating fluid theory with variable range) to improve the calculation of repulsion interaction between the segments. The resulted model (SAFT-VR Mie EOS) is applied to *n*-alkane series and showed a significant improvement on the description of the compressed liquid phase, vapor−liquid equilibria and also estimation of thermo-physical properties. In order to get a full review on different type of SAFT versions and recent improvement in each field we refer the reader to Müller and Gubbins.[32] In current study, SAFT1, because of its accuracy, predictive capabilities and suitability for both vapor and liquid phases, is utilized to model the solubility and density of CO_2 in water with respect to SO_2 impurities. Therefore, our intention in this work is (1) to provide a reliable molecular model for H_2O + SO_2 + CO_2 mixture using the SAFT1 EoS, and (2) to check the capability of this variation of SAFT compare with other versions with respect to number of adjustable parameter.

The rest of the paper is organized as follows: section 2 contains a short summary of SAFT framework and some features of SAFT1; sections 3 and subsequent subsections (3.1−3.3) are devoted to describing of model for pure molecules and binary systems; model predictions for ternary system are presented in section 3.4; to end with, section 4 withdraws some concluding remarks.

2. MOLECULAR MODEL AND THEORY

Since all other thermodynamic properties can be estimated through Helmholtz free energy, SAFT-type EoS's are usually formulated in term of Helmholtz energy. Taking into the account the fact that most of the fluids are "real", a reliable EoS is one that more precisely estimates the deviation of Helmholtz energy of the system from ideal state (i.e., molecules with zero size and without interaction) due to different types of nonidealities. Hence, the residual molar Helmholtz energy at constant temperature and density is defined as

$$a^{res}_{(T,\rho,n)} = a_{(T,\rho,n)} - a^{ideal}_{(T,\rho,n)} \quad (1)$$

Helmholtz energy of a system is fundamentally calculated based on the potential energy of interacting molecules (i.e pair-potential). Within the SAFT framework, the residual Helmholtz energy (i.e., Helmholtz energy divided by *RT*) is composed of two parts:

$$a^{res} = \underset{reference}{a^{hs}} + \underset{perturbation}{a^{dis} + a^{chain}} + a^{assoc} \quad (2)$$

The reference term, in principle, could be any fluid with known residual Helmholtz energy and radial distribution function. Then, the existing radial distribution function of the reference fluid can be used to calculate the perturbation terms which are incremental Helmholtz energy due to chain formation (a^{chain}) or association (a^{assoc}). The simplest intermolecular potential which has characteristics of a reference fluid is hard-sphere (HS) potential which is used in the earlier version of SAFT.[16,17] Helmholtz energy of HS fluid(a^{hs})—which takes into the account the repulsive forces between the molecules− has been determined empirically by Carnahan and Starling.[33] In order to make the SAFT framework more

dx.doi.org/10.1021/jp505562j | J. Phys. Chem. B 2014, 118, 10214−10223

predictive there has been lots of research to improve the reference term via assigning different reference fluids like Lennard-Jones (LJ), square-well (SW) etc. The SAFT1 uses a square-well (SW) potential as a reference fluid. The square-well (SW) fluid defines by a steep repulsion at short distances and a short-ranged attraction at intermediate distances through three parameters: radial distance between two segments (r), the well depth (u), and the reduced range of the potential well (λ). The potential energy for two interacting spherical SW segments with contact distance (σ) is given by

$$\varphi(r) = \begin{cases} \infty & r < \sigma \\ -u\sigma \le r \le \lambda\sigma \\ 0 & r > \lambda\sigma \end{cases} \tag{3}$$

This potential energy (reference term in eq 1) is composed of two parts (1) the hard-sphere potential and (2) the perturbation given by the well depth (u) to capture short-range attraction between molecules. Adidharma and Radosz[19] incorporated Barker Henderson's perturbation scheme to account for incremental Helmholtz energy due to dispersion-(a^{dis}), i.e., the second part in eq 1. According to SAFT1, molecules are chains composed of (m) spherical segments of equal size bonded tangentially together and interacting via a square-well (SW) intermolecular potential. Therefore

$$\tilde{a}^{reference} = \tilde{a}^{SW} = \sum_i X_i m_i [\tilde{a}_0^{hs} + \tilde{a}_1^{disp} + \tilde{a}_2^{disp} + \tilde{a}^t] \tag{4}$$

X_i is the mole fraction of chain (i), $\tilde{a}_0^{hs}$ is the dimensionless hard-sphere Helmholtz energy per segment $\tilde{a}_{1,2}^{disp}$ is the first and second perturbation terms based on the Barker Henderson's perturbation scheme, and $\tilde{a}^t$ is a correction term which account for truncation error of second order perturbation theory. The incremental residual Helmholtz energy due to the chain formation can be estimated using the SW radial distribution function $g_{\alpha\beta}^{SW}$ as

$$\tilde{a}^{chain} = -\sum_i X_i (m_i - 1)[\ln g_i^{-SW}(\sigma_{\alpha\beta}) - \ln g_{0,i}^{-SW}(\sigma_{\alpha\beta})] \tag{5}$$

where ($\sigma_{\alpha\beta}$) is the distance between canters of segment α and β at contact and g_i^{-SW} is defined as

$$\ln g_i^{-SW}(\sigma_{\alpha\beta}) = \sum_{\beta \ge \alpha} B_{\alpha\beta,i} \ln g_{\alpha\beta}^{SW}(\sigma_{\alpha\beta}) \tag{6}$$

where ($B_{\alpha\beta,i}$) is the bond fraction of type $\alpha\beta$ in molecule of component (i). In case of homosegment chains this value is equal to unity. The $g_{0,i}^{-SW}$ is g_i^{-SW} evaluated at zero density.

$$g_{0,i}^{-SW}(\sigma_{\alpha\beta}) = 1 + u_{\alpha\beta}/T \tag{7}$$

The association term is calculated by Adidharma and Radosz[34] for square well fluids as

$$\tilde{a}^{assoc} = \sum_i X_i \sum_\alpha \left[\sum_{A_i \in \Gamma_i} \left(\ln X^{A_i} - \frac{X^{A_i}}{2} \right) + \frac{n(\Gamma_i)}{2} \right] \tag{8}$$

where $n(i)$ is the number of association sites on molecule i and X^{Ai} is the mole faction of molecules i not bonded at site A_i given by

$$X^{A_i} = (1 + \rho_n \sum_j [X_j \sum_{B_j \in \Gamma_j} (X^{B_j} \Delta^{A_i B_j})])^{-1} \tag{9}$$

where ρ_n is the number density and $\Delta^{A_i B_j}$ is the association strength between site A_i at molecule i and site B_j at molecule j. For detail explanation of these equations, we refer the reader to the original paper.[34] Having calculated the residual Helmholtz energy using SAFT1, all other necessary functions to calculate the phase equilibria and thermodynamic properties can be easily derived. For example, in order to evaluate vapor−liquid equilibria (VLE), equality of fugacity of all components in both phases is required. The fugacity can be estimated based on derivatives of residual Helmholtz energy respect to composition as

$$\ln \hat{\varphi}_i = \tilde{a}^{res} + \left(\frac{\partial \tilde{a}^{res}}{\partial x_k} \right)_{T,\rho,x_{i\neq k}} - \sum_{j=1} x_j \left(\frac{\partial \tilde{a}^{res}}{\partial x_j} \right)_{T,\rho,x_{i\neq k}} + Z - 1 - \ln Z \tag{10}$$

where Z is the compressibility factor, calculated with

$$Z = 1 + \rho \left(\frac{\partial \tilde{a}^{res}}{\partial \rho} \right)_{T,x} - 1 \tag{11}$$

Since the compressibility factor is function of density, iteration over density is required. However, convergence requires little iteration and in general SAFT is computationally quite cheap. The SAFT1 approach performs the phase equilibria calculation through number of cross interaction parameters for binary subsystems which account for the interactions between unlike segments in the mixture. For example, longitudinal distance segment α and β ($\sigma_{\alpha\beta}$) and reduced range of the potential well for the α−β interaction ($\lambda_{\alpha\beta}$) are calculated by Lorentz arithmetic mean. However, for well depth of square-well potential ($u_{\alpha\beta}$), geometric mean alongside a deviation parameter ($k_{\alpha\beta}$) (binary interaction parameter) is suggested:

$$u_{\alpha\beta} = u_{\beta\alpha} = \sqrt{u_\alpha u_\beta}(1 - k_{\alpha\beta}) \tag{12}$$

The binary interaction parameter has been found to be temperature dependent[8,35] and is usually determined through comparison against experimental data at different pressures and temperatures. It is worth mentioning that, chemical reactions and kinetic associated with mutual solubility of water in vapor phase and gases in the liquid phase is not our concern here. Moreover, it is assumed that the association term can capture the polarity contribution of the molecules.

3. RESULTS AND DISCUSSION

Considering local geothermal gradients, temperatures in the saline aquifers typically varies between 30−100 °C (303.15−373.15 K). In addition, to keep CO_2 under supercritical state (due to high density and low viscosity) it is usually injected at depths greater than 800 m. Assuming hydrostatic pressure gradients, the reservoir pressure for CO_2 storage candidates (depths >800 m) is about ∼6−30 MPa (60−300 bar). In this work we have covered these pressure−temperature window and also SO_2 composition from 0 to 80%.

In order to evaluate the phase state—the number of phases and corresponding composition—and thermodynamic properties of chemical species, the SAFT1 approach requires number of intermolecular parameters to be prespecified. The model requires four parameters for each compound, namely: (m), the segment number, (v_{oo}), the volume of the SW sphere, (λ), the reduced range of the potential well and (ε), the interaction

dx.doi.org/10.1021/jp505562j | J. Phys. Chem. B 2014, 118, 10214−10223

Table 1. SAFT1 Fitted Parameters for H_2O, CO_2, and SO_2

molecule/parameter	m	v^{00} (cm^3/mol)	u/k (K)	λ	ε/k (K)	κ
H_2O[28]	1.0000	9.483 70	313.8758	1.5423	1527.72	0.058 48
CO_2[35]	1.2126	11.5845	230.4929	1.5390	581.432	0.006 336
SO_2	2.0283	9.525 74	219.4379	1.6061	200.720	0.318 000

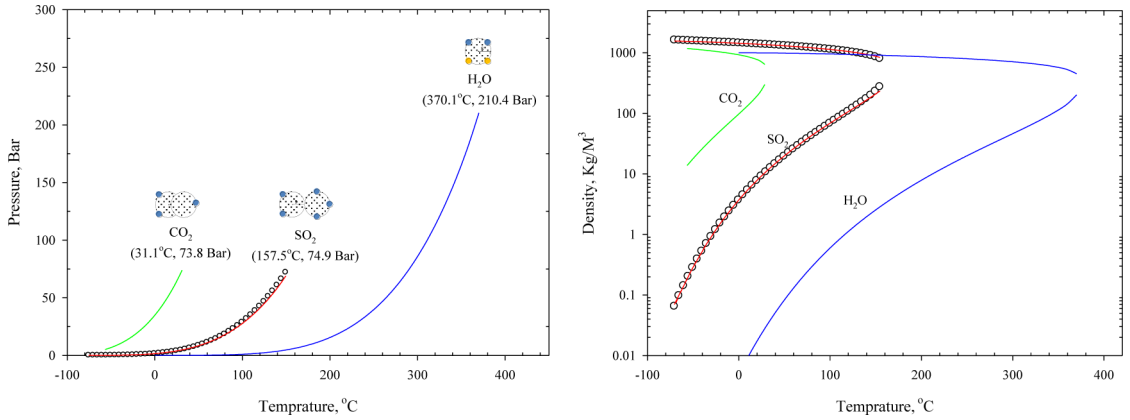

Figure 1. Fitted EOS for (a) vapor pressure and (b) coexisting vapor and liquid densities of SO_2, CO_2, and H_2O. Continuous lines are SAFT1 predictions and open circles are experimental data.[44] The approximate molecular geometries used by SAFT1 are also shown along with critical pressure and temperatures in this figure.

energy of the segment.[19,34] For associative molecules, two additional parameters are needed, the association volume (κ^{AB}) and the well depth of the association site−site potential (ε^{AB}). Some of these parameters can be estimated from first-principles calculations. For instance, Singh et al.[36] and Leonhard et al.[37] have incorporated quantum mechanics principles—*ab intio* and density functional theory—to obtain the molecular parameters for PCP-SAFT. However, the most common method is fitting the experimentally obtained saturated liquid densities and vapor pressures against the model. Phase behaviors of some pure components and also binary mixtures, all relevant to this study, have been previously described with SAFT1 (CO_2,[35] H_2O,[28] NaCl−H_2O,[35] CO_2−H_2O,[35] and CO_2−H_2O−NaCl[35]) in wide range of thermodynamic condition with excellent accuracy except near the critical point.

One reason for SAFT1 over predictions in the vicinity of critical point is due to clustering of molecules and consequently large density fluctuation. This physical behavior is not included in SAFT1 or other classical equation of state.[19] One solution to describe the thermodynamics of a system near the critical region is to use scaling laws with universal crossover functions. Another way to overcome this obstacle is by rescaling the conformal parameters to the experimental critical temperature and pressure.[38] Nevertheless, we use sets of adjusting parameters obtained for CO_2 and H_2O. We refer the reader to the original papers for complete results of these subsystems and also list of the pure components adjusting parameters (m, v_{oo}, λ, κ^{AB}, and ε^{AB}). In the following sections the other subsystem has been studied by the model and adjusting parameters has been derived.

In this study we have incorporated three components (SO_2, CO_2, and H_2O) and consequently three segments in the modeling algorithm. The model for water molecules in this study is based on the four-site single segment model used by Tanet al.,[39] in which two associating site of type (H) and type (O) represent the proton-donor sites and electron loan pairs, respectively. Two sites of the same type (i.e., O−O or H−H) do not associate. It is worth to mention that, cross association between unlike sites (i.e., O−H) represent the hydrogen bonding. CO_2 is modeled as linear molecule with two hard-sphere segments which are bonded tangentially together.[35] The large quadropoles moment of CO_2 allows this molecule to associate with itself or other molecule in the mixture. There are four electron loan pairs in the CO_2 molecule which can contribute to hydrogen bonding, however, our examination on CO_2 with different numbers of association sites showed that three association schemes will gives best fit to experimental vapor pressure and density. Therefore, we accept two associating site of type (O) and one site of type(C) for CO_2 molecule. Again, sites of the same type (i.e., O−O and C−C) do not associate with each other.

SO_2 is a symmetrical nonlinear molecule with a large dipole moment (1.6 D) and high polarity. There are four electron loan pairs in the oxygen atoms of the molecule and one extra loan pair in the sulfur atom. These electron loan pairs are allowed to provide association site for proton-donor sites (hydrogen atoms) and therefore contribute to hydrogen bonding. In case of SO_2 four association site of type (S) and one site of type (O) are considered. For associating subsystems in this study system, estimation of fractions of nonbonded molecules is not analytically possible; therefore we have implemented a generalized procedure recently proposed by Tanet al.[40] to evaluate the association term. It is worth to mention that the polar and quadropoles interactions of water, carbon dioxide and sulfur dioxide are considered by the association (hydrogen-bonding-type) interaction.

3.1. Pure Components (SO_2/CO_2/H_2O). The SAFT1 parameters of pure SO_2 are fitted to its vapor pressure and saturated liquid density from 197 to 427 K. The experimental data were taken from the National Institute of Standards and Technology (NIST) online database.[44] A trust region Levenberg−Marquardt algorithm is incorporated in order to fit the experimental data to the theory. The fitting results are shown in Table 1 and Figure 1 together with previously

dx.doi.org/10.1021/jp505562j | J. Phys. Chem. B 2014, 118, 10214−10223

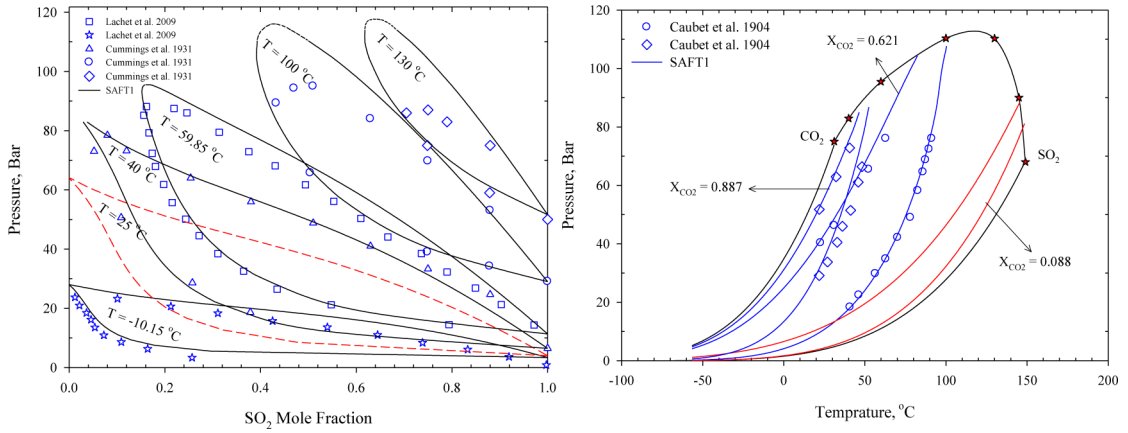

Figure 2. Predicted (a) pressure−composition projection of phase diagram for binary mixture of SO_2 and CO_2 at different temperatures and (b) pressure−temperature phase diagram of SO_2 and CO_2 at fixed composition. Continues lines are SAFT1 predictions and symbols are experimental data.[11−13] The red dotted curves are the SAFT1 pure predictions.

obtained results for water and carbon dioxide. As shown in Figure 1 the prediction agrees with the experimental data, except near the critical point (which is due to density fluctuation not included in the model). The average relative deviations (ARDs) for the vapor pressure and liquid density are 2.7% and 0.92%, respectively. ARD is calculated by

$$\mathrm{ARD} = \frac{1}{NP}\sum_{N=1}^{NP}\left(\left|1 - \frac{P_N^{cal}}{P_N^{\exp}} \text{ or } \frac{\rho_N^{cal}}{\rho_N^{\exp}}\right|\right) \times 100 \qquad (13)$$

Considering the assumed number of association sites, once the experimental data are fitted to the SAFT1, then an approximation of molecule geometry can be drawn (Figure 1). On the basis of our estimation, SO_2 is a molecule composed of two segments and five association sites. In addition, volume available for association (κ^{AB}) in SO_2 is much larger than that of CO_2 which could elucidate the higher solubility of SO_2 in water.

3.2. SO_2−CO_2 Binary Mixture. The experimental data on vapor−liquid equilibria (VLE) of this system is very rare. For the SO_2−CO_2, vapor liquid equilibria has been measured by Cummingset al.[12] at 40, 100, and 130 °C and pressure from 0 up to 12 MPa. Similar experiments have also been performed by Lachetet al.[13] at −10.15 and 59.85 °C, where a fairly good consistency of data is observed comparing with molecular simulation using the Gibbs Ensemble Monte Carlo method. Figure 2a shows the SAFT1 estimation of SO_2−CO_2 mixture VLE at aforementioned temperatures, compare with experimental data. The model predictions at 25 °C are also demonstrated in the graph with the red line. The results show a satisfactory agreement without using any binary interaction coefficient, although in the previous study using PC-SAFT and CPA a three-parameter temperature dependent coefficient is used to fit the experimental data.[8]

For SO_2−CO_2 mixture, at temperatures less than the critical temperature of CO_2 (30.85 °C), a phase split is happening in the whole SO_2 concentration range. However, as temperature increases the size of the two phase region decreases (consequently, a wider safe operation window) and a phase split occurs only if the SO_2 concentration exceeds a critical value. Moreover, at a given temperature, bubble and dew point pressures have steady downward trends with increasing SO_2, which impose a lower minimum pressure with respect to transportation. On the other hand, as temperature rises, the critical pressure is steady increasing reaching a peak at ∼110 °C and then drops toward the critical temperature of the SO_2. This behavior is further illustrated in Figure 2b, where the critical locus of SO_2−CO_2 mixture, obtained from previous calculations, is plotted alongside with saturation pressure curves of the pure components. Continues critical locus with one maximum is a characteristic of phase behavior of type I fluids, based on the phase equilibria classification proposed by Galindo et al.[41] This type of fluids present weak intermolecular interactions which further justify using zero binary interaction coefficient between CO_2 and SO_2. In addition, in this pressure−temperature (PT) diagram, the theory predictions in case of ∼12, 38 and 92% SO_2 impurities are shown to be in a very good agreement with experimental data.[11] Our estimations show that, inclusion of 5−10% of SO_2 could change the critical pressure and temperature approximately 0.7−2 MPa and 10−30 °C, respectively. In case of reservoirs with thermodynamic state close to the critical point, these variations in temperature and pressure are unfavorable as the system enters into the two-phase region.

Density of CO_2−SO_2 mixture is of significant importance on the side of CCS processes, since it has direct relation with pressure propagation, amount of CO_2 that can be stored and plume migration velocity. An attempt was made to predict the coexisting densities of the mixture at 25, 40, 60, 100, and 130 °C. The results are illustrated in Figure 3, where pure CO_2 coexisting densities are also plotted for the sake of comparison. Only available experimental data at ∼60 °C are also plotted.[13] Both liquid and gas densities predicted by the SAFT1 are in excellent agreement with experimental data. At low pressures, the equilibrium liquid density decreases as temperature increases, whereas the opposite is valid at higher pressures. In addition, the critical density of the CO_2−SO_2 mixture is increasing with temperature, and at higher temperatures the value (∼600 kg.m^{-3}) is much greater than pure CO_2 (∼460 kg.m^{-3}).

With a view to understand effect of SO_2 impurity, using the same set of adjusting parameters and without any further readjustment, densities of single phase CO_2−SO_2 mixtures were predicted at temperatures of 25, 40, 100, and 200 °C and pressure up to 30 MPa. The results are presented in Figure 4a−d. The dash lines in the figure show the two-phase region (phase split). Continues lines represent the density of fluid as it starts from the gas phase at low pressure and then passes

dx.doi.org/10.1021/jp505562j | J. Phys. Chem. B 2014, 118, 10214−10223

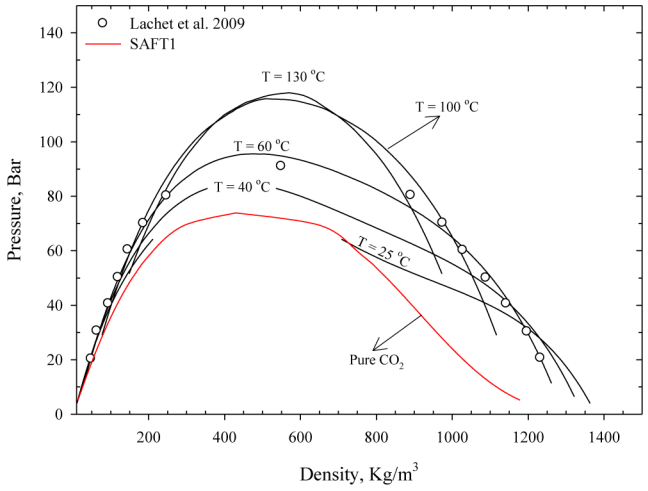

Figure 3. Equilibrium densities of binary mixture of SO_2 and CO_2 at different temperatures. Symbols are experimental data,[13] and the curves are SAFT1 calculations.

through two-phase or critical region and finally ends up in the dense phase. The predictions indicate that with increasing SO_2 concentrations, the density of SO_2−CO_2 mixture has always an increasing upward trend throughout the whole range pressures up to 30 MPa. Higher density of mixtures improves the efficiency and safety of transportation and therefore inclusion of SO_2 is favorable with respect to transportation. Moreover, as density of injected fluid increases the gravity override or buoyancy forces which control the migration of plume toward the cap rock is reduced. So, in one hand the risk of CO_2 leakage is moderates while storage capacity of reservoir increasers. To explore in more detail the effect of sulfur dioxide in the phase behavior and density of carbon dioxide, we have performed additional calculation at higher temperatures. At 100 °C the phase split take place when the concentration of SO_2 is greater than 40% and this critical value decreases with increasing temperature.

3.3. SO_2−H_2O Binary Mixture. Equilibrium solubility of SO_2 in pure water is measured and reported by several researchers. We have plotted these data on the PT diagram of Figure5. Unfortunately, information on the high pressure solubility and also density of aqueous solution are very rare. Solubility of SO_2 in water at different temperatures and up to 2.5 MPa is calculated and plotted against experimental data.[42] The results are presented in Figure 6. In this study, we have considered only one type of cross-association, i.e., between the site of type (O) in SO_2 and the site of type (H) in H_2O. One should notice that pure SO_2 and H_2O association mechanism is not same. The latter is due to hydrogen bonding, i.e. association between unlike sites of type (H) and type (O). While association interaction between unlike sites of type (O) and (S) in SO_2 is not hydrogen bonding. Therefore, to capture cross-association between water and SO_2 or CO_2, Jiet al.[35] suggested that instead of using the common mixing rules, one should directly fit the cross-association parameters (i.e., κ^{AB},

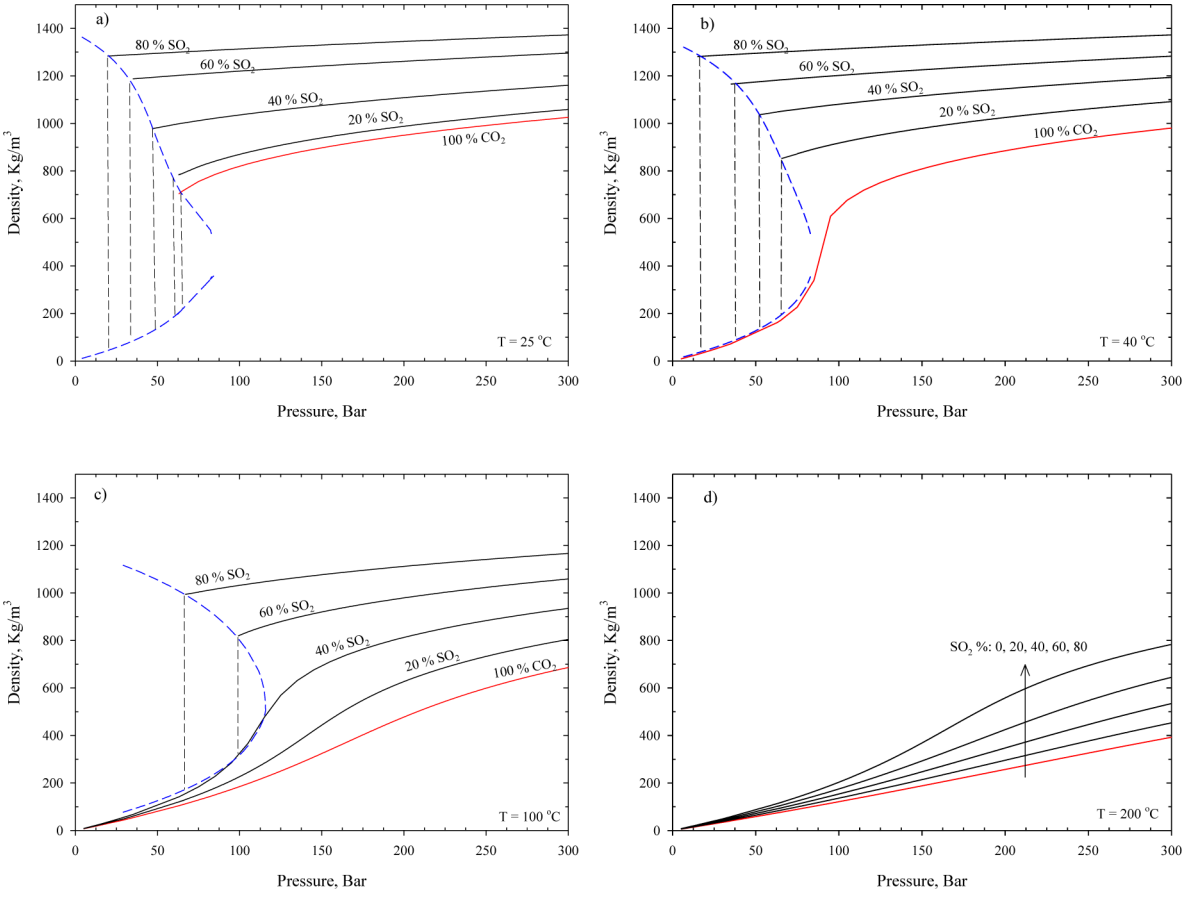

Figure 4. Density of CO_2−SO_2 mixture at 25, 40, 100, and 200 °C and different concentration of SO_2. The black dash lines represent the phase split and the blue dash lines are the equilibrium densities.

dx.doi.org/10.1021/jp505562j | J. Phys. Chem. B 2014, 118, 10214−10223

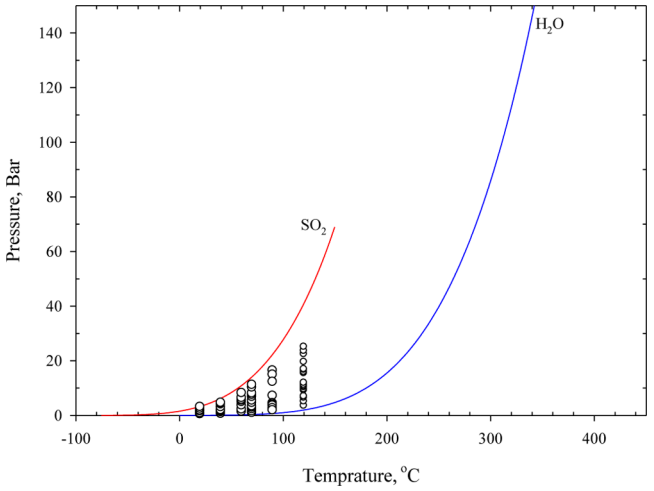

Figure 5. Pressure−temperature projection of SO_2−H_2O phase diagram. The open circles are the experimental data used in this study. The solid curves are saturation pressure of pure components.

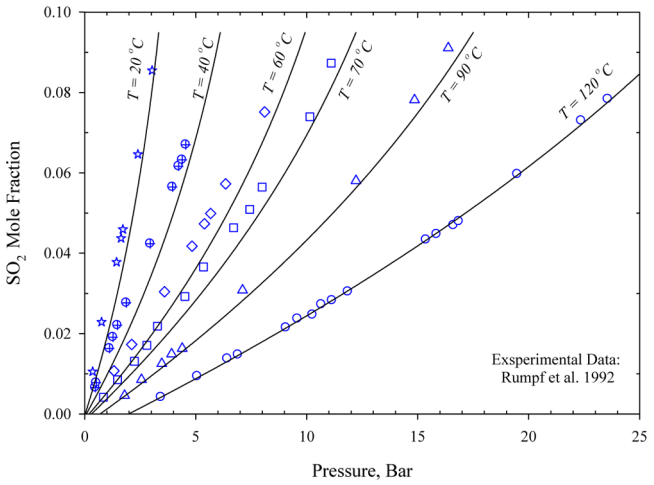

Figure 6. Pressure−composition projection of SO_2−H_2O phase diagram at 25, 40, 60, 70, 90, and 120 °C. The solid curves are SAFT1 predictions and the symbols are experimental data[42]

ε^{AB}) to the experimental data. Their results showed that these adjusting parameters are functions of temperature and they used a four degree polynomial to model this dependency. In this study we used the common mixing rule for the association well depth (i.e., ε^{OH} =565 K) between unlike sites. However, κ^{OH}, which is a measure of the volume available for bonding between sites (H) in water and type (O) in SO_2, is found to be slightly greater (~0.169) the value obtained using the available mixing rule(~0.153). In addition we confirmed that at higher temperatures (>90 °C) a slighter higher value of κ^{OH} (~0.17) gives a better prediction, however this dependency is very small and can be neglected.

As these results shows, at a given temperature and pressure, SO_2 solubility in water is much higher than CO_2 at same thermodynamic condition. Moreover, the trend of the solubility curve is not like that of CO_2. As pressure increases, the rate of the increase in SO_2 solubility is increasing toward the liquid−liquid equilibria whereas CO_2 solubility curve experience a gradually decreasing rate. In another word, pressure act as an intensifier agent in case of SO_2, which might be due to higher probability of self-association at higher pressures.

Vapor liquid equilibria (mutual solubilities) of the system at 100 °C are also experimentally measured by Spall et al.[43] Theory predictions using SAFT1 are compared with these experimental data in Figure 7. As this figure confirms, both

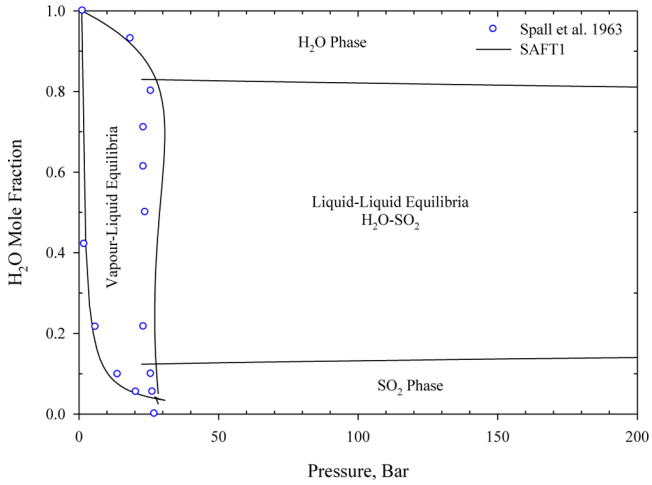

Figure 7. Pressure−composition projection of SO_2−H_2O phase diagram at 100 °C. The solid curves are SAFT1 predictions, and the symbols are experimental data[43]

estimated SO_2 solubility in water and water content of SO_2 are remarkably fit with experiment. The solubility of water in the SO_2 is almost same as CO_2 in the water in the VLE region, whereas at higher pressures, in the liquid−liquid equilibria (LLE) region the water content is considerably higher. Moreover, the discontinuity between VLE and LLE is much more pronounced here which shows high degree of immiscibility between SO_2 and water. Therefore, a discontinues critical locus line, such as for the CO_2−H_2O case, is expected which is a characteristic of phase behavior of type III fluids.[41] There is also equilibrium between two liquids and one vapor phase in the middle region in Figure 7. Modeling of phase equilibria associated with this region is complicated and needs a three phase flash calculation module. Our calculations in this region are very close to the reality however still more improvement is necessary.

3.4. CO_2−SO_2−H_2O Ternary Mixture. In case of ternary CO_2−SO_2−H_2O mixtures, we have performed some additional calculation at temperatures 50, 75, and 100 °C and pressures up to 30 MPa, with different SO_2 concentrations all applicable to reservoir condition. The calculated solubility of the CO_2 + SO_2 in water and corresponding aqueous densities are illustrated in Figure 8. It is shown that with increasing SO_2, the total solubility of the gas mixture (CO_2 + SO_2) increases at all temperatures and for the whole range of pressures. The corresponding mass densities show increasing upward trends too. The growth rate of total gas solubility and also mass density has an exponential behavior i.e. rate of growth is proportional to the concentration of SO_2. It is worth to mention that negative effect of temperature on CO_2 solubility is preserved with inclusion of SO_2, however, at higher temperatures rate of decay is higher compare with pure CO_2. Moreover, transition from VLE to LLE (the discontinuities in the figures) only occurs when certain amount of SO_2 is included to the mixture, for example, at 50 °C with 60% SO_2 and at 75 °C with 80% SO_2. Another remarkable conclusion that can be deduced form these calculations, is the very modest

dx.doi.org/10.1021/jp505562j | J. Phys. Chem. B 2014, 118, 10214−10223

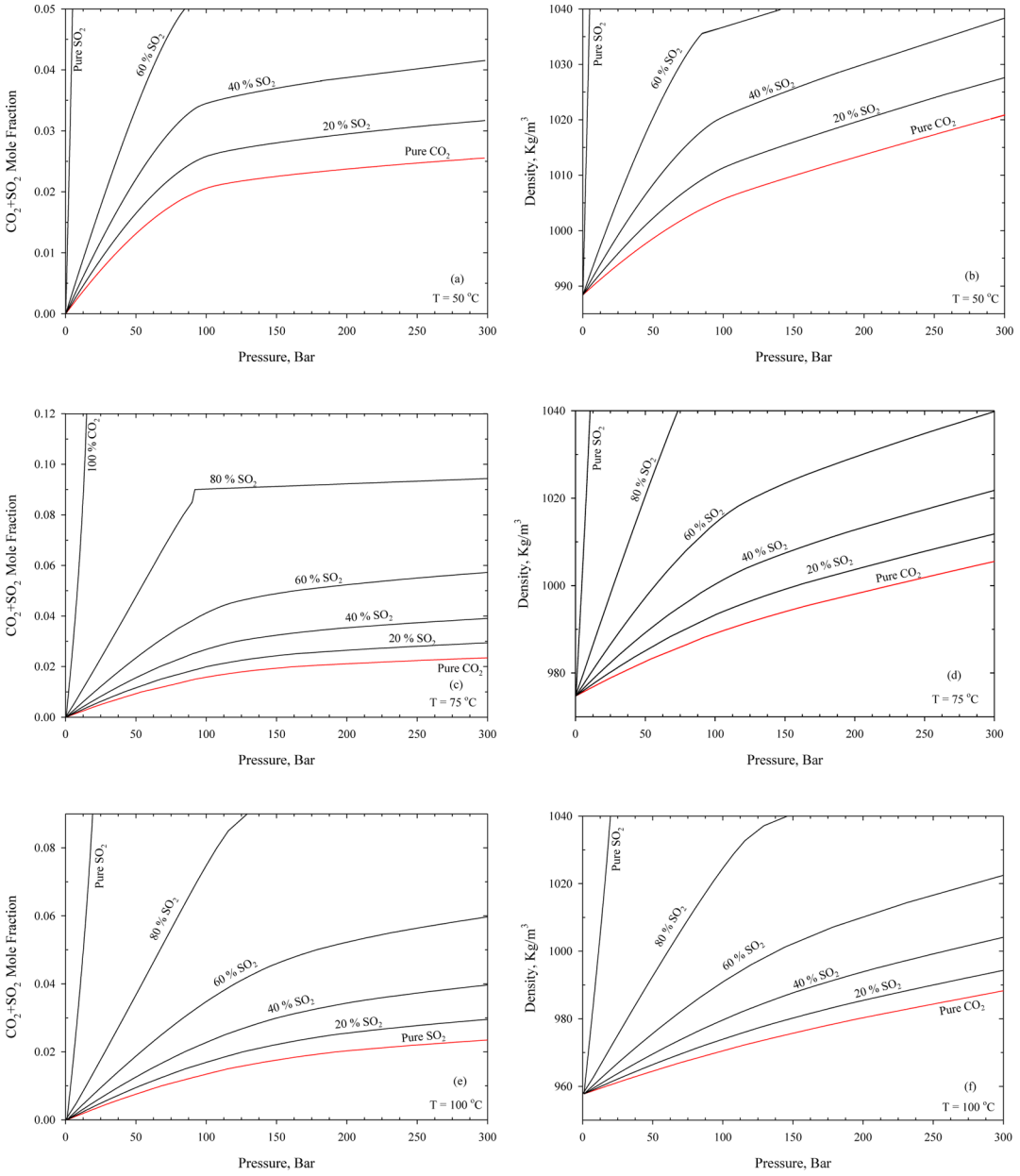

Figure 8. Solubility of the SO_2−CO_2 gas mixture in the water at 50, 75, and 100 °C and corresponding aqueous mass density at different SO_2 concentrations. The solid curves are SAFT1 predictions.

effect of SO_2 on the total gas solubility and density at small concentration of SO_2. In other word, if the concentration of SO_2 impurity in the injected gas stream is less than 5% the total change in gas solubility is negligible. This effect in more detail is illustrated in Figure 9 at 50 °C and 10 MPa. The CO_2 concentration is almost constant for SO_2 concentrations less than 50% and then has a very small downward trend, while the SO_2 solubility increases. This confirms that (1) total gas solubility is dominated by the solubility of SO_2 and (2) SO_2 has a very negligible effect on the solubility of CO_2.

4. CONCLUSIONS

Having knowledge of the phase behavior of ternary CO_2−SO_2−H_2O mixtures over a wide range of pressures and temperatures is required with respect to a CCS process, as SO_2 might affect very much the transportation efficiency, geochemistry of fluid-rock systems and even operational concerns like injectivity. To the best of our knowledge no experimental data on solubility and density of aqueous ternary CO_2−SO_2−H_2O mixture are available in the literature (due to the highly corrosive nature of the system). Therefore, our main intention for doing this research is to provide a reliable molecular model for H_2O + SO_2 + CO_2 mixture using the SAFT1 EoS. The SAFT framework is chosen due to (1) high nonideal interactions of the molecule in this system and (2) promising predictive capabilities.

Comparison of the results of SAFT1 model against the available experimental data of binary systems demonstrated the capability of this equation of state on modeling of such a complex system, although, in contrast to the previous works, no temperature dependent binary interaction coefficient is used. Only in the case of the SO_2−H_2O set, the volume available for bonding between unlike sites requires a little adjustment. This adjustment is found to largely improve handling the

dx.doi.org/10.1021/jp505562j | J. Phys. Chem. B 2014, 118, 10214−10223

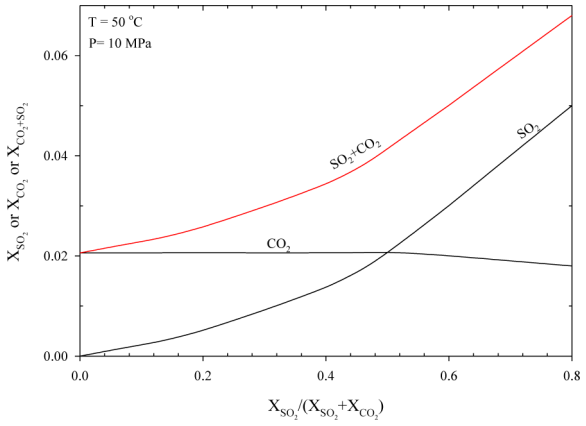

Figure 9. Equilibrium composition of CO_2–SO_2–H_2O at 50 °C and 10 MPa calculated by SAFT1. "*X*" represent the mole fraction.

discontinuity between VLE and LLE due to high degree of immiscibility. Moreover, our estimation shows that inclusion of SO_2 to the CO_2 stream may shift the PT diagram to the higher pressure–temperature region. For example having 5–10% SO_2 in the injected stream could change the critical pressure and temperature by approximately 0.7–2 MPa and 10–30 °C, respectively. The modeling also shows that the mass density of SO_2–CO_2 mixtures has an increasing upward trend throughout the whole range pressures up to 30 MPa. Finally, the total solubility of CO_2 in water varies exponentially with respect to SO_2 concentrations. This implies that, if the concentration of SO_2 impurity is approximately less than 5%, which is the case in many CCS applications, then the variation of CO_2 solubility in water is negligible.

AUTHOR INFORMATION

Corresponding Authors

*(R.M.) E-mail: rohaldin.miri@geo.uio.no.

*(H.H.) E-mail: helge.hellevang@geo.uio.no.

Notes

The authors declare no competing financial interest.

ACKNOWLEDGMENTS

Dr. Hertanto Adidharma and Dr. Sugata Tan have provided invaluable help in making and discussing the solver for the SAFT equations. This work was (partly) funded by the Research Council of Norway and industry partners through the project 190002/S60 Subsurface storage of CO_2—Injection well management during the operational phase (Inject). This work has also been partly funded by the University of Oslo and the SUCCESS Centre for CO_2 storage under Grant 193825/S60 from the Research Council of Norway (RCN).

REFERENCES

(1) Wigley, T. M.; Richels, R.; Edmonds, J. A. Economic and environmental choices in the stabilization of atmospheric CO_2 concentrations. *Nature* **1996**, *379*, 240–243.

(2) Houghton, J. T.; Ding, Y.; Griggs, D. J.; Noguer, M.; van der Linden, P. J.; Dai, X.; Maskell, K.; Johnson, C. *Climate change 2001: the scientific basis*; Cambridge University Press: Cambridge, U.K., 2001; Vol. *881*.

(3) Bruant, R. G.; J, Jr.; Celia, M. A.; Guswa, A. J.; Peters, C. A. Peer Reviewed: Safe Storage of CO_2 in Deep Saline Aquifiers. *Environ. Sci. Technol.* **2002**, *36* (11), 240A–245A.

(4) Benson, S. M.; Orr, F. M. Carbon dioxide capture and storage. *MRS Bull.* **2008**, *33* (04), 303–305.

(5) Metz, B.; Davidson, O.; De Coninck, H.; Loos, M.; Meyerl L. *Carbon dioxide capture and storage*; Cambridge University Press: Cambridge, U.K., 2005

(6) Blanco, S. T.; Rivas, C.; Fernández, J.; Artal, M.; Velasco, I. Influence of Methane in CO_2 Transport and Storage for CCS Technology. *Environ. Sci. Technol.* **2012**, *46* (23), 13016–13023.

(7) Crandell, L. E.; Ellis, B. R.; Peters, C. A. Dissolution Potential of SO_2 Co-Injected with CO2 in Geologic Sequestration. *Environ. Sci. Technol.* **2009**, *44* (1), 349–355.

(8) Tan, S. P.; Yao, Y.; Piri, M. Modeling the Solubility of SO_2 + CO_2 Mixtures in Brine at Elevated Pressures and Temperatures. *Ind. Eng. Chem. Res.* **2013**, *52* (31), 10864–10872.

(9) Ziabakhsh-Ganji, Z.; Kooi, H. An Equation of State for thermodynamic equilibrium of gas mixtures and brines to allow simulation of the effects of impurities in subsurface CO_2 storage. *Int. J. Greenhouse Gas Control* **2012**, *11*, S21–S34.

(10) Sayegh, S.; Najman, J. Phase behavior measurements of CO2-SO2-brine mixtures. *Can. J. Chem. Eng.* **1987**, *65* (2), 314–320.

(11) Caubet, F. The liquifaction of gas mixtures. *Z. Kompr. Fluess. Gase Pressluft-Ind.* **1904**, *8*, 65.

(12) Cummings, L. W. T. High-pressure rectification. *Ind. Eng. Chem.* **1931**, *23* (8), 900–902.

(13) Lachet, V.; De Bruin, T.; Ungerer, P.; Coquelet, C.; Valtz, A.; Hasanov, V.; Lockwood, F.; Richon, D. Thermodynamic behavior of the CO2+ SO2 mixture: Experimental and Monte Carlo simulation studies. *Energy Procedia* **2009**, *1* (1), 1641–1647.

(14) Li, H.; Yan, J. Evaluating cubic equations of state for calculation of vapor–liquid equilibrium of CO2 and CO2-mixtures for CO2 capture and storage processes. *Appl. Energy* **2009**, *86* (6), 826–836.

(15) Fu, D.; Feng, J.; Lu, J. Bulk and Interfacial Properties for CO2-SO2 Binary Mixtures. *Chin. J. Chem.* **2010**, *28* (10), 1885–1889.

(16) Chapman, W. G.; Gubbins, K. E.; Jackson, G.; Radosz, M. SAFT: Equation-of-state solution model for associating fluids. *Fluid Phase Equilib.* **1989**, *52*, 31–38.

(17) Huang, S. H.; Radosz, M. Equation of state for small, large, polydisperse, and associating molecules. *Ind. Eng. Chem. Res.* **1990**, *29* (11), 2284–2294.

(18) Zhou, Q.; Birkholzer, J. T.; Tsang, C.-F.; Rutqvist, J. A method for quick assessment of CO2 storage capacity in closed and semi-closed saline formations. *Int. J. Greenhouse Gas Control* **2008**, *2* (4), 626–639.

(19) Adidharma, H.; Radosz, M. Prototype of an engineering equation of state for heterosegmented polymers. *Ind. Eng. Chem. Res.* **1998**, *37* (11), 4453–4462.

(20) Zhao, H.; Morgado, P.; Gil-Villegas, A.; McCabe, C. Predicting the Phase Behavior of Nitrogen + n-Alkanes for Enhanced Oil Recovery from the SAFT-VR Approach: Examining the Effect of the Quadrupole Moment. *J. Phys. Chem. B* **2006**, *110* (47), 24083–24092.

(21) Llovell, F.; Florusse, L. J.; Peters, C. J.; Vega, L. F. Vapor–Liquid and Critical Behavior of Binary Systems of Hydrogen Chloride and n-Alkanes: Experimental Data and Soft-SAFT Modeling. *J. Phys. Chem. B* **2007**, *111* (34), 10180–10188.

(22) Andreu, J. S.; Vega, L. F. Modeling the Solubility Behavior of CO2, H2, and Xe in [C n-mim][Tf_2N] Ionic Liquids. *J. Phys. Chem. B* **2008**, *112* (48), 15398–15406.

(23) Kroon, M. C.; Karakatsani, E. K.; Economou, I. G.; Witkamp, G.-J.; Peters, C. J. Modeling of the carbon dioxide solubility in imidazolium-based ionic liquids with the tPC-PSAFT equation of state. *J. Phys. Chem. B* **2006**, *110* (18), 9262–9269.

(24) Paduszyński, K.; Domańska, U. Thermodynamic Modeling of Ionic Liquid Systems: Development and Detailed Overview of Novel Methodology Based on the PC-SAFT. *J. Phys. Chem. B* **2012**, *116* (16), 5002–5018.

(25) Gross, J.; Sadowski, G. Perturbed-chain SAFT: An equation of state based on a perturbation theory for chain molecules. *Ind. Eng. Chem. Res.* **2001**, *40* (4), 1244–1260.

(26) Gross, J.; Sadowski, G. Modeling polymer systems using the perturbed-chain statistical associating fluid theory equation of state. *Ind. Eng. Chem. Res.* **2002**, *41* (5), 1084−1093.
(27) Ji, P.; Feng, W.; Tan, T.; Zheng, D. Modeling of water activity, oxygen solubility and density of sugar and sugar alcohol solutions. *Food Chem.* **2007**, *104* (2), 551−558.
(28) Tan, S. P.; Adidharma, H.; Radosz, M. Statistical associating fluid theory coupled with restricted primitive model to represent aqueous strong electrolytes. *Ind. Eng. Chem. Res.* **2005**, *44* (12), 4442−4452.
(29) Ji, X.; Zhu, C. Predicting possible effects of H_2S impurity on CO_2 transportation and geological storage. *Environ. Sci. Technol.* **2012**, *47* (1), 55−62.
(30) Lafitte, T.; Bessieres, D.; Piñeiro, M. M.; Daridon, J.-L. Simultaneous estimation of phase behavior and second-derivative properties using the statistical associating fluid theory with variable range approach. *J. Chem. Phys.* **2006**, *124* (2), 024509.
(31) Lafitte, T.; Piñeiro, M. M.; Daridon, J.-L.; Bessières, D. A comprehensive description of chemical association effects on second derivative properties of alcohols through a SAFT-VR approach. *J. Phys. Chem. B* **2007**, *111* (13), 3447−3461.
(32) Müller, E. A.; Gubbins, K. E. Molecular-based equations of state for associating fluids: A review of SAFT and related approaches. *Ind. Eng. Chem. Res.* **2001**, *40* (10), 2193−2211.
(33) Carnahan, N. F.; Starling, K. E. Equation of state for nonattracting rigid spheres. *J. Chem. Phys.* **1969**, *51* (2), 635−636.
(34) Adidharma, H.; Radosz, M. SAFT1 for associating fluids: Alkanols. *J. Phys. Chem. B* **2001**, *105* (40), 9822−9827.
(35) Ji, X.; Tan, S. P.; Adidharma, H.; Radosz, M. SAFT1-RPM approximation extended to phase equilibria and densities of CO_2-H_2O and CO_2-H_2O-NaCl systems. *Ind. Eng. Chem. Res.* **2005**, *44* (22), 8419−8427.
(36) Singh, M.; Leonhard, K.; Lucas, K. Making equation of state models predictive: Part 1: Quantum chemical computation of molecular properties. *Fluid Phase Equilib.* **2007**, *258* (1), 16−28.
(37) Leonhard, K.; Van Nhu, N.; Lucas, K. Making equation of state models predictive: Part 2: An improved PCP-SAFT equation of state. *Fluid Phase Equilib.* **2007**, *258* (1), 41−50.
(38) Míguez, J.; Dos Ramos, M.; Piñeiro, M.; Blas, F. An examination of the ternary methane + carbon dioxide + water phase diagram using the SAFT-VR approach. *J. Phys. Chem. B* **2011**, *115* (31), 9604−9617.
(39) Tan, S. P.; Ji, X.; Adidharma, H.; Radosz, M. Statistical associating fluid theory coupled with restrictive primitive model extended to bivalent ions. SAFT2:1. single salt + water solutions. *J. Phys. Chem. B* **2006**, *110* (33), 16694−16699.
(40) Tan, S. P.; Adidharma, H.; Radosz, M. Generalized procedure for estimating the fractions of nonbonded associating molecules and their derivatives in thermodynamic perturbation theory. *Ind. Eng. Chem. Res.* **2004**, *43* (1), 203−208.
(41) Galindo, A.; Whitehead, P. J.; Jackson, G. Predicting the high-pressure phase equilibria of water + *n*-alkanes using a simplified SAFT theory with transferable intermolecular interaction parameters. *J. Phys. Chem.* **1996**, *100* (16), 6781−6792.
(42) Rumpf, B.; Maurer, G. Solubilities of hydrogen cyanide and sulfur dioxide in water at temperatures from 293.15 to 413.15 K and pressures up to 2.5 MPa. *Fluid Phase Equilib.* **1992**, *81*, 241−260.
(43) Spall, B. Phase equilibria in the system sulphur dioxide-water from 25−300 °C. *Can. J. Chem. Eng.* **1963**, *41* (2), 79−83.
(44) Burgess, D. R. *Thermochemical Data. NIST Chemistry WebBook*; NIST Standard Reference Database Number 69; Linstrom, P.J., Mallard, W.G., Eds.; National Institute of Standards and Technology: Gaithersburg MD, http://webbook.nist.gov, (retrieved March 25, 2014).